Data-Driven Driving State Control for Unmanned Agricultural Logistics Vehicle

XUESHENG ZHOU AND **JUN ZHOU**
College of Engineering, Nanjing Agricultural University, Nanjing 210095, China
Corresponding author: Jun Zhou (lanzhouwangna@163.com)

ABSTRACT Logistic activities widely exist in the agricultural production process. With the gradual application of unmanned technology in agricultural production, the technology related to intelligent logistics has become a research hotspot. Because of the complicated driving road conditions of agricultural logistics vehicles, vehicle stability control has become a key problem for realizing intelligent driving. In this paper, the control of unmanned agricultural logistics vehicles in complex farmland environment is studied to provide data support for the intelligent driving of agricultural vehicles. In the current paper, based on the characteristics of the four-wheel drive independent control moment response of distributed electric agricultural vehicle, a coordinated stability control method based on the improved adaptive model predictive control (MPC) is proposed. In the paper, an unmanned agricultural logistics vehicle platform is developed. The front and rear radars mounted on the platform is used to scan the targets and obstacles in the operation site, and a relevant target and position coordinate database is established to provide data support for the intelligent driving of agricultural logistics vehicles. In the paper, the information base established by the front and rear radar scanning can control the driving attitude and path of the agricultural logistics transportation platform and realize the intelligent agricultural logistics.

INDEX TERMS Logistic activities, unmanned driving technology, agricultural big data structure, model predictive control.

I. INTRODUCTION

The distributed electrically driven vehicle has multiple power units, each of which is independent and controllable, so that it can coordinate and control the driving force based on the current road condition to ensure the stability of vehicle handling. The idea of coordinated control is especially important when the vehicle exhibits drive failure, drive slip, etc. [1]–[4]. Conventional electric agricultural vehicles have only a single power source. When the agricultural vehicle has drive failure, drive slip, etc., it is unable to perform multi-drive unit coordination control. The general treatment is to reduce the torque of the drive motor or shut down the motor, which makes it quickly stop. In the event of drive failure and drive slip, the distributed electrically driven vehicle can satisfy the driver's needs through the coordinated control of redundant power sources to ensure effective, safe and smooth driving of the vehicle.

The basic principle of front- and rear-wheel drive regulation based on economy is given by Kondo *et al.* [5]. This method holds that under different working conditions, different driving modes (front/rear) should be adopted to improve the economy. The front wheel should be used in the normal driving process, the four-wheel drive mode should be used in case of wheel sliding and steering before starting, and the four-wheel braking mode should be used in the deceleration and braking conditions to recover as much energy as possible.

In case of motor drive failure, one solution for handling motor failure would shut down both the failed driving wheel and the contralateral driving wheel [6]–[8]. Although this method can guarantee a part of the driving capacity in the case of single-wheel failure or coaxial dual-wheel failure, it can not perform real-time torque distribution control according to the current vehicle state. In addition, both partial motor failure and lack of motor response speed were not considered by the method, which weakens the longitudinal driving performance of the vehicle and fails to completely solve the problem of reasonable driving under the failure condition.

The associate editor coordinating the review of this manuscript and approving it for publication was Zhiwu Li.

The rule-based control allocation method was applied to address the excessive slip condition [9]. In the case of single-wheel or multiple-wheel sliding, the method transferres the driving torque of the sliding wheel to the non-sliding wheel, which satisfies the longitudinal driving performance and transverse stability of the vehicle. However, the method is only suitable for the over-slip condition, and it does not provide a comprehensive solution, which is used to solve the problem of the drive failure driven slip and direct yaw moment control.

From the current research situation, in the distributed electric vehicle driving force coordination control system, the lateral control target cannot well reflect the driver's demand [10]. At present, most studies have focused on how to follow multiple motion control targets, yaw angular velocity and lateral deflection of the centre of mass of the vehicles [11]–[15], but the nonlinear characteristics of the vehicles have not been fully considered, and the adaptive adjustment of control targets is lacking. In the paper, a control method is designed to adjust the control target according to the current vehicle and environment after the vehicle enters the strong nonlinear region, and the vehicle can follow the adjusted control target in real time to ensure stability.

The operation environment of agricultural logistics vehicles is complicated, and the road surface is changeable, which makes the vehicle driving control especially important. At present, the driving control of agricultural transport vehicles mainly focuses on the estimation of road adhesion coefficient, and there is no systematic research on the control mode. In addition, the research on intelligent driving and attitude control is even less. Currently, the research on agricultural vehicles remains in the traditional driving mode, and the research on attitude control and the intelligent driving of agricultural vehicles is limited [16]–[18]. In the current paper, aiming at the development of distributed drive electric agricultural logistics vehicles, an unmanned test and control equipment is built. Using the real-time target and obstacle coordinate information database, the distributed electrically driven agricultural vehicle drive coordination control method with improved adaptive MPC is adopted to realize the intelligent operation of agricultural vehicle.

II. THE ESTABLISHMENT OF MODEL
A. THE BASIC MODEL OF THE VEHICLE SYSTEM
Since the stability of the vehicle is closely related to its lateral and yaw motion, the vehicle with the front-wheel steering was simplified into a two-degree-of-freedom model without considering the difference in steering angle of the front wheel [19], [20], as shown in Fig. 1.

The vehicle dynamic characteristics can be derived from vehicle dynamics theory, as follows:

$$\dot{\beta} = \frac{F_{yf} + F_{yr}}{mV} - \gamma \tag{1}$$

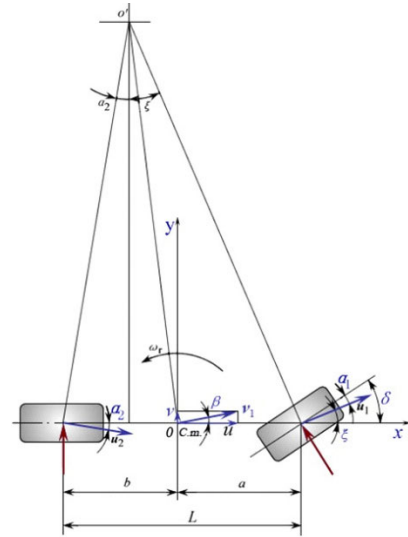$$\dot{r} = \frac{L_f F_{yf} - L_r F_{yr} + M_z}{I_z} \tag{2}$$

FIGURE 1. Two-degree-of-freedom model of vehicles.

The yaw moment M_z generated by the longitudinal force of the wheel can be calculated by the following formula:

$$M_z = \frac{d}{2} \cdot (-F_{xfl} + F_{xfr} - F_{xrl} + F_{xfl}) \tag{3}$$

The differential equations of the linear two-degree-of-freedom vehicle model are as follows:

$$\begin{cases} (k_1 + k_2)\beta + \frac{1}{v_x}(ak_1 - bk_2)r - k_1\delta_f = m(\dot{v}_y + v_x\gamma) \\ (ak_1 - bk_2)\beta + \frac{1}{v_x}(a^2 k - b^2 k_2)r - ak_1\delta_f = I_Z\dot{r} \end{cases} \tag{4}$$

where k_1 and k_2 are the lateral stiffness of the front and rear shafts of the linear two-degree-of-freedom model.

When information such as the steering wheel angle input and speed is known, according to the two-degree-of-freedom model, the steady-state values of the lateral deflection angle of the centre of mass and the yaw angular velocity can be obtained as follows:

$$r_d = \frac{v_x/L}{1 + Kv_x^2}\delta_f \tag{5}$$

$$\beta_d = \frac{b + amv_x^2/k_2 L}{(1 + Kv_x^2)/L}\delta_f \tag{6}$$

where

$$K = \frac{m}{L^2}\left(\frac{a}{k_2} - \frac{b}{k_1}\right) \tag{7}$$

$$r_{d\_bound} = 0.85\frac{ug}{v_x} \tag{8}$$

$$|\beta_{d\_bound}| \le \tan^{-1}(0.02\mu g) \tag{9}$$

The reference model of predictive control of the vehicle system is as follows:

$$\dot{x} = Ax + Bu \tag{10}$$

$$y(t) = Cx \tag{11}$$

where

$$A = \begin{bmatrix} \dfrac{k_1 + k_2}{mv_x} & -1 + \dfrac{-bk_2 + ak_1}{mv_x^2} \\ \dfrac{-bk_2 + ak_1}{I_z} & \dfrac{-b^2k_2 + a^2k_1}{I_z v_x} \end{bmatrix} \quad (12)$$

$$B = \begin{bmatrix} -\dfrac{k_1}{mv_x} & 0 \\ -\dfrac{ak_1}{I_z} & \dfrac{1}{I_z} \end{bmatrix} \quad (13)$$

$$C = \begin{bmatrix} 1 & 0 \\ 0 & 1 \end{bmatrix} \quad (14)$$

$$x = \begin{bmatrix} \beta \\ \gamma \end{bmatrix} \quad (15)$$

$$u = \begin{bmatrix} \delta \\ T \end{bmatrix} \quad (16)$$

The predictive control model includes two processes: rolling optimization and feedback correction [21], [22]. The prediction model is continuously optimized by rolling; simultaneously, the optimization process uses the measured information for continuous feedback correction, and the predicted output value is given to make the predicted value as close as possible to the expected value. In the vehicle movement process, the model predictive control is beneficial for enhancing the robustness of the control system in the predicted time domain because the driving environment greatly changes, and there are many uncertainties [23]–[25]. The predicted output value is obtained by optimizing the expected value as the optimization objective. At each sampling moment, the optimization is repeated, which is the rolling optimization.

B. PREDICTIVE CONTROL ALGORITHM BASED ON THE ADAPTIVE MODEL

First, equation (10) is discretized as follows:

$$x(k + 1) = A_1 x(k) + B_1 u(k) \quad (17)$$

where A_1 and B_1 are the coefficient matrices of the discrete system, and their expansion is expressed as follows:

$$A_1 = \sum_{I=0}^{\infty} \frac{A_1^i t_s^i}{i!} \quad (18)$$

$$B_1 = \sum_{i=0}^{\infty} \frac{B_1^i t_s^i}{i!} \quad (19)$$

The control inputs u, system state x, and system output y are defined as follows:

$$u = \begin{bmatrix} \delta_f \\ T_{cfl} \\ T_{cfr} \\ T_{crl} \\ T_{crr} \end{bmatrix} \quad (20)$$

$$x = \begin{bmatrix} \beta \\ \gamma \\ k_{fl} \\ k_{fr} \\ k_{rl} \\ k_{rr} \end{bmatrix} \quad (21)$$

$$y = \begin{bmatrix} \beta \\ \gamma \end{bmatrix} \quad (22)$$

where fl, fr, rl and rr are four different wheels: left front, left rear, right front and right rear, respectively.

The state equation of the control stability of the distributed drive agricultural vehicles is as follows:

$$\dot{x}_1 = \frac{F_{yf}(x_1, x_2, u_1) + F(x_1, x_2)}{mV} - x_2 \quad (23)$$

$$\dot{x}_2 = \frac{L_f \cdot F_{yf}(x_1, x_2, u_1) - L_r F_{yr}(x_1, x_2) + M_z}{mV} \quad (24)$$

$$\dot{x}_i = (-\frac{R_e^2}{JV} - \frac{x_i + 1}{\frac{1}{4}mV_x})C_{ki}x_i + \frac{R_e}{JV}u_{i-1},$$
$$i = 3, 4, 5, 6 \quad (25)$$

$$M_z = \frac{d}{2}(-C_{kfl}x_3 + C_{kfr}x_4 - C_{krl}x_5 + C_{krr}x_6) \quad (26)$$

$$\begin{cases} \min J(U) = \sum_{j=1}^{n} \sum_{i=1}^{p} \left[y_{rj}(k + i) - y_{pj}(k + i)^2 \right] \\ \quad + \sum_{l=1}^{m} \sum_{r=1}^{M} \lambda_1 \left[\Delta u_1(k + r - 1) \right]^2 \\ s.t. \ U_{\min} \le U \le U_{\max} \end{cases} \quad (27)$$

$$\begin{cases} \min J_1 = \sum_{j=1}^{N} \left[y_{j|k} - y_{j|k}(\theta) \right]^2 + \gamma \sum_{i=1}^{n\theta} (\Delta\theta_{i|k})^2 \\ s.t. \ \{U_{\min} \le U \le U_{\max} \end{cases} \quad (28)$$

C. OPTIMAL CONTROLLER DESIGN BASED ON MPC

The control input u is as follows: $U(k) = \{u_1(k), u_2(k), \cdots u_m(k)\}$.

The system output y is as follows: $Y(k) = \{y_1(k), y_2(k), \cdots y_n(k)\}$

At moment k, $E(k)$ is defined as the output reference sequence including β_r and γ_r.

The key to maintaining the lateral stability of the vehicle is to generate the yaw moment acting on the vehicle by coordinating the driving torque [26]–[28]; thus, the horizontal tracking deviation is minimized.

Thus:

$$\min J(U) = \sum_{i=1}^{P} \left[(\beta(k + i) - \beta_r(k))^2 \cdot H_1 + (\gamma(k + i) \right. $$
$$\left. - \gamma_r(k)^2) \cdot H_2 \right] \quad (29)$$

$$J(U) = \sum_{j=1}^{n} \sum_{i=1}^{P} [\beta(k + i) - \beta_r(k)]^2 \cdot H_1$$
$$+ \sum_{l=1}^{m} \sum_{r=1}^{M} (\gamma(k + i) - \gamma_r(k)^2) \cdot H_2 \quad (30)$$

where n and m are dimensions of the controlled quantity and controlled quantity, P is the predictive horizon, M is the control horizon, and $P \geq M$. $\beta(k+i) - \beta_r(k)$ is the tracing deviation of the sideslip angle; $\gamma(k+i) - \gamma_r(k)$ is the tracing deviation of the yaw velocity; H_1 and H_2 are the positive weighted coefficient of adjusting tracking performance; H=diag(H_1, H_2) is the weighting matrix.

D. ONLINE ROLLING OPTIMIZATION OF THE DRIVE COORDINATION SYSTEM UNDER CONSTRAINT CONDITIONS

Agricultural vehicles in a complex environment may appear to have large swing due to the external interference. The stability of the system is affected by excessive yaw angle [29], [30]. Thus, the yaw angle constraint must be considered.

$$\|\phi(k+i)\|_2^2 \leq \phi_{max}^2, \quad i \geq 1 \tag{31}$$

According to the predictive control theory of the model, to enable the vehicle to stably run, performance indicators as shown in equations (29) and (30) must be optimized. The optimal control increment that satisfies discrete state equations and system constraints ΔU is obtained. Finally, an optimal control sequence $\{U^*(k), U^*(k+1), \cdots U^*(k+M-1)\}$ is obtained. The optimal control input vector includes an active steering angle and four motor driving torques. Only the first control $U^*(k)$ of the optimal control sequence can be applied to the system.

$$\min J(U) = \sum_{j=1}^{n}\sum_{i=1}^{P}[\beta(k+i) - \beta_r(k)]^2 \cdot H_1$$
$$+ \sum_{l=1}^{m}\sum_{r=1}^{M}(\gamma(k+i) - \gamma_r(k)^2) \cdot H_2$$
$$s.t. \ U_{min} \leq U \leq U_{max} \tag{32}$$

E. MODEL PREDICTIVE FEEDBACK CORRECTION

In practice, the performance of the control system is easily affected by external interference, model mismatch, etc. Feedback correction can predict the error and timely correct it through output compensation. In other words:

$$E(k) = Y(k) - Y_n(k) \tag{33}$$
$$Y(k+i) = Y_n(k+i) + \lambda E(k) \tag{34}$$

where λ is the compensation coefficient. Feedback information plays an important role in the process of predictive control and forms a closed loop optimization.

F. SOLUTION OF THE NONLINEAR PREDICTIVE CONTROL LAW BASED ON THE SEQUENTIAL QUADRATIC PROGRAMMING (SQP) OPTIMIZATION

The core of the NMPC is the nonlinear constrained optimization problem. Different controller structures can be obtained using different optimization strategies. In addition, the optimization strategy has important influence on the control

effect, adaptability and robustness of the predictive control. Because the established prediction model is relatively complex, the solution speed is very slow if the traditional intelligent optimization algorithm is adopted, whereas the sequential quadratic programming (SQP) algorithm is one of the most effective methods to solve nonlinear constrained optimization problems with global convergence and superlinear convergence speed. SQP is faster than GA and PSO in solving the predictive control law.

The basic idea of the SQP algorithm is as follows: at a certain approximate solution, the original nonlinear programming problem is simplified to a simple quadratic programming problem, and an optimal solution is obtained. If the solution is so, the optimal solution of the quadratic programming problem is considered the optimal solution of the original nonlinear programming problem [31], [32]. Otherwise, a new quadratic programming problem is constructed by the approximate solution, and the iteration continues.

The optimal control law in equations (29) and (30) is expressed as a nonlinear constraint optimization as follows:

$$\begin{cases} \min J(U) = \sum_{j=1}^{n}\sum_{i=1}^{P}[\beta(k+i) - \beta_r(k)]^2 \cdot H_1 \\ + \sum_{l=1}^{m}\sum_{r=1}^{M}(\gamma(k+i) - \gamma_r(k)^2) \cdot H_2 \\ s.t. f_i(U) \leq 0 \end{cases} \tag{35}$$

$f_i(U)$ is a vector team of function with inequality constraints in equations (29) and (30).

The specific steps to solve equation (35) using the SQP algorithm are as follows:

First Step: The Lagrangian multiplier λ_i is introduced; then, the Lagrangian function of equation (35) is as follows:

$$L(U, \lambda) = J(U) + \sum_{i=1}^{m}\lambda_i f_i(U) \tag{36}$$

Second Step: At iteration point U^k, equation (35) is transformed into the following quadratic programming subproblem:

$$\begin{cases} \min \frac{1}{2}d^T H_k d + \nabla J^T(U^k)d \\ s.t. \ \nabla f_i^T(U^k)d + f(U^k) \leq 0 \end{cases} \tag{37}$$

where H_k is Hessian matrix of equation (36) at $U = U^k$.

Third Step: By solving the quadratic programming problem of equation (37), the next search direction d^k can be obtained, and the next iteration point can be updated.

$$U^{k+1} = U^k + \varepsilon_k d^k \tag{38}$$

Fourth Step: The BFGS algorithm is used to update the Hessian matrix of Lagrangian function.

$$
\begin{cases}
H_{k+1} = H_k + \dfrac{q_k q_k^T}{q_k^T q} - \dfrac{H_k^T s_k s_k^T H_k}{s_k^T H_k s_k} \\
s_k = U_{k+1} - U_k \\
q_k = \nabla J(U_{k+1}) + \displaystyle\sum_{i=1}^{m} \lambda_i \nabla f_i(U_{k+1}) \\
\quad - \left[\nabla J(U_k) + \displaystyle\sum_{i=1}^{m} \lambda_i \nabla f_i(U_k) \right]
\end{cases} \tag{39}
$$

Fifth Step: When the solution satisfies the termination condition, $\left| U^{k+1} - U^k \right| \le \delta$. In the paper, when the given accuracy δ is 10^{-6}, U^{k+1} can be considered the optimal control law U^*.

G. ADAPTIVE PREDICTIVE CONTROL PARAMETER UPDATING

The accuracy of the nonlinear prediction model is affected by the external interference and various uncertainties [33]–[36]. To reduce the error between the output of the actual system and the output of the prediction model and obtain good predictive control performance, the model parameter adaptive estimator is introduced to realize the online adjustment of the parameter set of the prediction model [37]–[41].

$$
\begin{cases}
s.t. \begin{cases}
y_{j|k} = f_j(U(k-1), \cdots, U(k-l), \\
\qquad Y(k-1), \cdots Y(k-s)) \\
\hat{y}_{j|k}(\mu) = \displaystyle\sum_{i=1}^{l} r_{i,j} K_j(X, X_i) + b_j \\
\Delta \mu_{i|k} = \mu_i(k) - \mu_i(k-1)
\end{cases} \\
\min_{\mu} J_1 = \displaystyle\sum_{j=1}^{n} \left[y_{j|k} - \hat{y}_{j|k}(\mu) \right]^2 + \omega \sum_{i=1}^{n_\mu} \left(\Delta \mu_{i|k} \right)^2
\end{cases} \tag{40}
$$

where μ is parameters $r_{i,j}$ and b_j in the prediction model; $\omega > 0$ is the weight; n is the output dimension; i is the number of model parameters; $y_{j|k}$ is the j-dimensional output at k.

In equation (40), the unknown parameter vector μ is obtained by the gradient descent method to minimize the objective function. The initial value of the parameter vector is provided, and the parameter vector is updated using the following formula:

$$
\mu(k+1) = u(k) - \zeta \frac{\partial J_1}{\partial u} \tag{41}
$$

where $\zeta(0 < \zeta < 1)$ is the positive learning rate; $\frac{\partial J_1}{\partial u}$ is calculated as follows:

$$
\frac{\partial J_1}{\partial u} = -2 \sum_{j=1}^{n} [f_j(X) - \sum_{i=1}^{l} r_{i,j} K(X, X_i) - b_j] K(X, X_i)
$$
$$
+ 2\gamma \left[\Upsilon_{i,j} - \Upsilon_{i,j}(k-1) \right] \tag{42}
$$

When the iteration satisfies the termination condition, the parameter values of the prediction model after adaptive adjustment at the current time can be obtained.

III. SIMULATION TEST AND ANALYSIS

To verify the effect of the driving coordination control based on MPC and adaptive MPC on the driving stability of distributed electric agricultural logistics vehicles, simulation tests of continuous steering, double-shift line condition, and step steering were performed under the experimental conditions of low-adhesion road surfaces [42]–[46].

A. CONTINUOUS STEERING SIMULATION CONDITION

The simulation analysis is performed on electrically driven agricultural vehicles driving on low-adhesion roads with an operating speed of 15 km/h. When electric agricultural vehicles run at the operating speed on low-adhesion roads, they are prone to instability under continuous steering conditions. To verify the effectiveness of the designed driver coordination control strategy based on MPC and adaptive MPC, in the paper, the simulation conditions were set as shown in Table 1. The steering wheel angle input is shown in Fig. 2, and the simulation results are shown in Fig. 3 and Fig. 4.

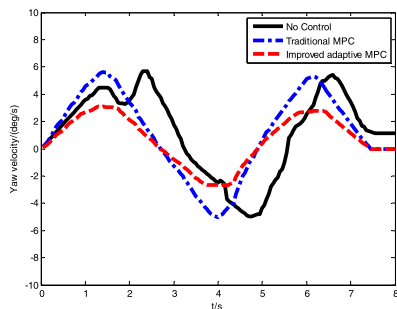**TABLE 1. Continuous steering condition.**

| Condition number	The description of conditions	Driving condition	Road adhesion coefficient
T1	Continuous steering	Running operation(15 km/h)	0.27
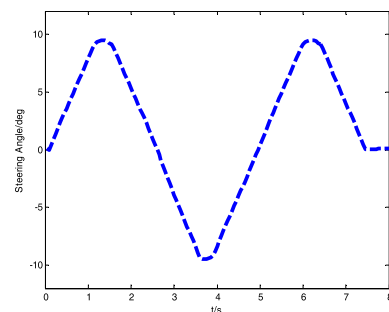
FIGURE 2. Continuous steering wheel angle input.

In the continuous steering simulation experiment, the T1 condition simulated the operating condition of agricultural vehicles on low-adhesion roads (muddy roads). The initial speed of the vehicle was 15 km/h, and the road adhesion coefficient was 0.27.

Fig. 3 and Fig. 4 show the variation process of the yaw angular velocity and lateral deviation angle of centre of mass under three control strategies based on MPC, adaptive MPC and no control strategy. As shown in Fig. 3 and Fig. 4,
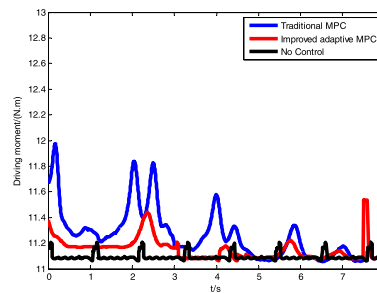
FIGURE 3. Curve of the yaw angular velocity under the continuous steering condition.
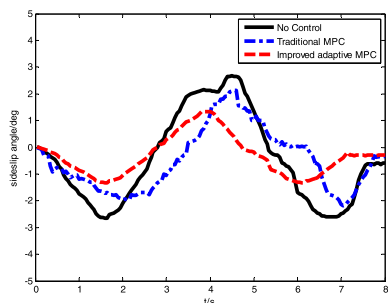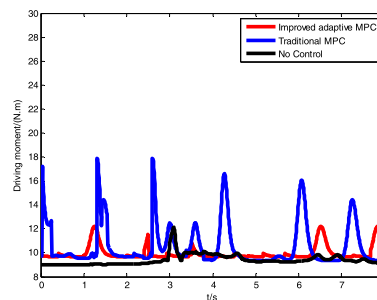

FIGURE 4. Curve of the lateral deviation angle of the centre of mass under the continuous steering condition.

FIGURE 5. Change curve of the driving torque of the left front wheel under the continuous steering condition.

FIGURE 6. Change curve of the driving torque of the right front wheel under the continuous steering condition.

FIGURE 7. Change curve of the driving torque of the left rear wheel under the continuous steering condition.

FIGURE 8. Change curve of the driving torque of the right rear wheel under the continuous steering condition.

in the case of continuous steering, the change range of the vehicle yaw angular velocity and lateral deviation angle of the centre of mass is minimized based on the adaptive MPC control, which keeps the driving attitude of agricultural logistics vehicles in a good state. The adaptive MPC control has an obviously better effect than the traditional MPC control. When there is no control strategy, agricultural logistics vehicles have obvious hysteresis when they continuously turn, such that they can not follow the steering command to adjust their position in time, which caused instability. As shown in Fig. 3, at 2-3 s, with no control strategy, the yaw angular velocity obviously changes from low to high step, which causes the vehicle to have an instantaneous yaw instability phenomenon and results in a greatly increased probability of vehicle instability and deviation from the established route. As shown in Fig. 4, at 3.5-4.5 s, when no control strategy is adopted, the variation of lateral deviation angle of the centre of mass obviously increases and is accompanied by a step change, which leads to the increase in probability of vehicle rolling and the increase in vehicle instability. In the course of the variation of the yaw angular velocity and lateral deviation angle of the centre of mass, there is always a steering problem and following hysteresis.
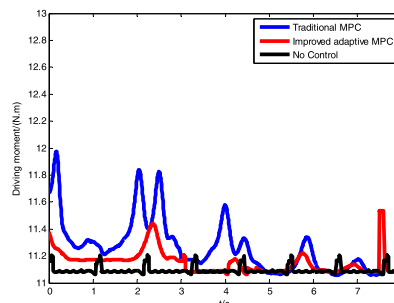
The change curves of the driving torque of each driving wheel under the continuous steering condition are shown in Figs. 5-8. Simultaneously, the vehicle operating conditions without failure, without coordinated control and with coordinated control are compared. During the simulation, the vehicle makes continuous 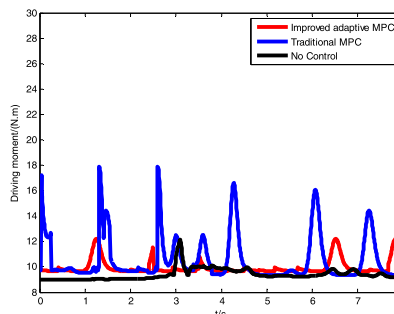steering according to the given steering instruction, and the required direct yaw moment is 0. When there is no control, the torque of each driving wheel is basically unchanged, and the vehicle continues to turn following the turn command in the entire process. However, the

excessive sliding of the driving wheels on the low-adhesion road surface makes the vehicle path deviate. The steering manoeuvrability can be improved by changing the driving torque of the left and right wheels at each steering time point using the traditional MPC control. The improved adaptive MPC control is adopted to adjust the torque changes of the left and right driving wheels at any time, which makes the continuous steering more coordinated and stable.

B. DOUBLE SHIFT LINE SIMULATION CONDITION

The simulation analysis on the double-shift line steering of electrically driven agricultural vehicles at the operating speed of 15 km/h on the low-adhesion road surface is performed. To verify the effectiveness of the designed driver coordination control strategy based on MPC and adaptive MPC in the current study, the simulation conditions are shown in Table 2 [47]–[50]. The steering wheel angle input is shown in Fig. 9.

TABLE 2. Double shift line steering condition.

| Condition number	The description of conditions	Driving condition	Road adhesion coefficient
T2	Double shift line steering	Running operation(15 km/h)	0.27
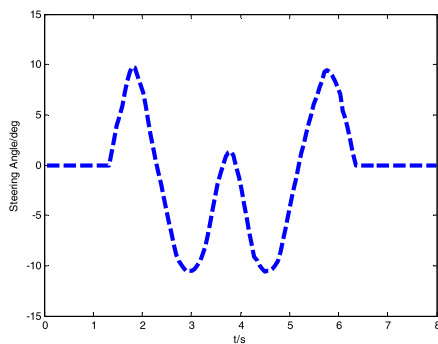
FIGURE 9. Double shift line steering wheel angle input.

In the double-shift line simulation experiment, the T2 condition simulated the operating condition of agricultural vehicles on low-adhesion roads and muddy roads. The initial speed of the vehicle is 15 km/h, and the road adhesion coefficient is 0.27, suggesting advantages in computer applications that are suitable for parallel computing.
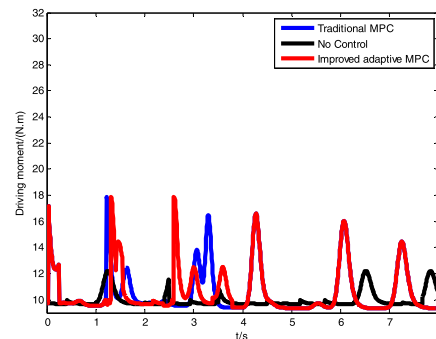
The change curves of the driving torque of each driving wheel under the condition of double-shift line are shown in Figs. 10-13. Similar to the continuous steering control
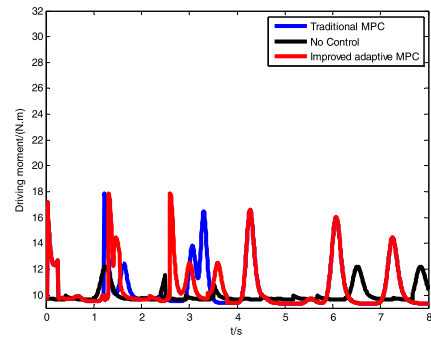
FIGURE 10. Change curve of the driving torque of the left front wheel under the double-shift line steering condition.
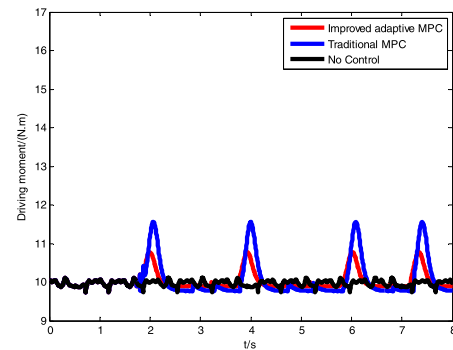
FIGURE 11. Change curve of the driving torque of the right front wheel under the double-shift line steering condition.

FIGURE 12. The change curve of the driving torque of the left rear wheel under double-shift line steering condition.

process, the improved adaptive MPC control can adjust the torque changes of the left and right driving wheels at any time to make the continuous steering more coordinated and stable, which is obviously better than the traditional MPC control. At each steering time point of the double-shift line, the accurate tracking of driving instructions was improved by controlling the changes in driving torques of the left and right wheels.

C. ANGULAR STEP STEERING SIMULATION CONDITION

When agricultural logistics vehicles are working in the field, they often need to perform sharp steering operation to complete the turn or change the operating area, and angular step
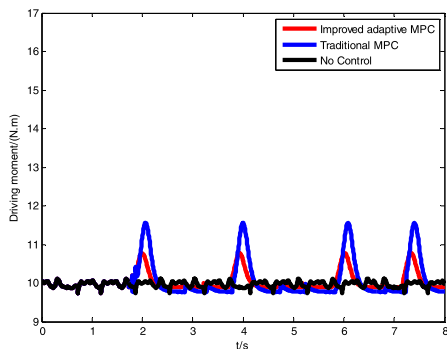
FIGURE 13. The change curve of the driving torque of the right rear wheel under double-shift line steering condition.

TABLE 3. Step steering condition.

Condition number	The description of conditions	Driving condition	Road adhesion coefficient
T3	Step steering	Running operation(15 km/h)	0.27
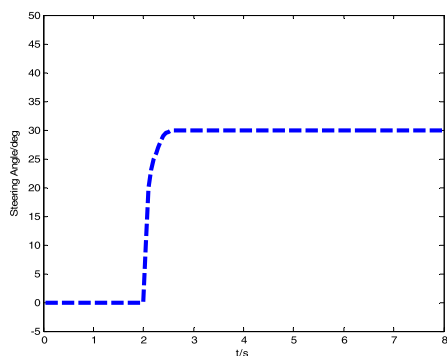
FIGURE 14. Angular step steering wheel corner input.

FIGURE 15. Curve of the yaw angular velocity under the step steering condition.
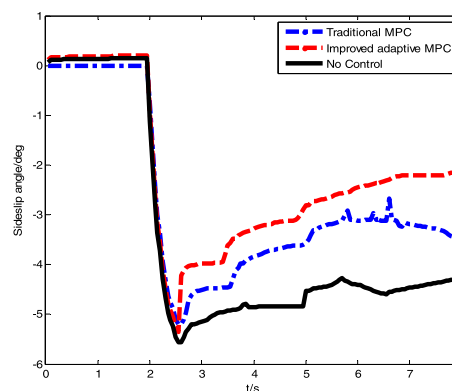
FIGURE 16. Curve of the lateral deviation angle of the centre of mass under the step steering condition.

steering input is selected to simulate this working condition. A step steering simulation analysis of electrically driven agricultural vehicles on low-adhesion road surface with operating speed of 15 km/h is performed. In the paper, the simulation conditions are set as shown in Table 3. The steering wheel angle input is shown in Fig. 14. The simulation results are shown in Fig. 15 and Fig. 16.

In the simulation experiment of angular step steering, the T3 condition simulated the operating condition of agricultural vehicles on low-adhesion road and muddy road. The initial speed of the vehicle is 15 km/h, and the road adhesion coefficient is 0.27.
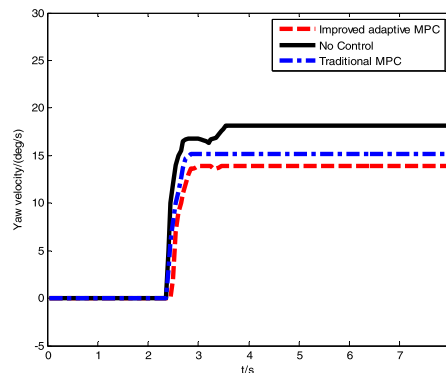
The variation process of the yaw angular velocity and lateral declination of the centre of mass based on MPC, adaptive MPC and no control strategy is shown in Figs. 15 and 16. At the step turn, both conventional MPC control and adaptive MPC control can reduce the variation range and overshoot of the yaw rate and side-slip angle of the mass centre. Compared to not using any control strategy, to a large extent, the stability of the lateral swing and roll during step steering and the smaller steering radius are guaranteed by using the conventional MPC control and adaptive MPC control. The manoeuvrability of step steering is improved.

The change curves of the driving torque of each driving wheel under the condition of step steering are shown in Figs. 17-20. As shown in Figs. 17 and 19, during step steering, the torque of the left-side drive, inside wheel, and wheels of agricultural vehicles gradually decrease from 3 s and subsequently gradually increase as the steering proceeds. When there is no control, the reduction in speed and amplitude of the drive torque of the inside drive wheel is smaller, and the driving torque of the outer wheel increases with less speed and amplitude. Thus, step steering is not complete, which results in path deviation. When using traditional MPC and improved adaptive MPC control, the driving force of the inner drive wheel can be largely reduced in time with
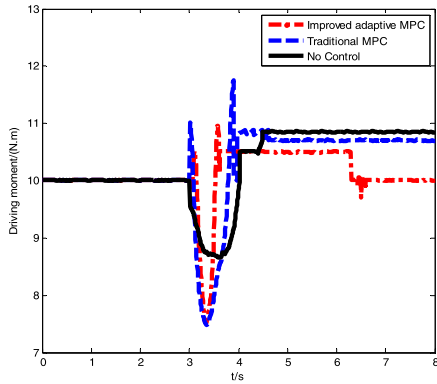
FIGURE 17. Change curve of the driving torque of the left front wheel under the step steering condition.
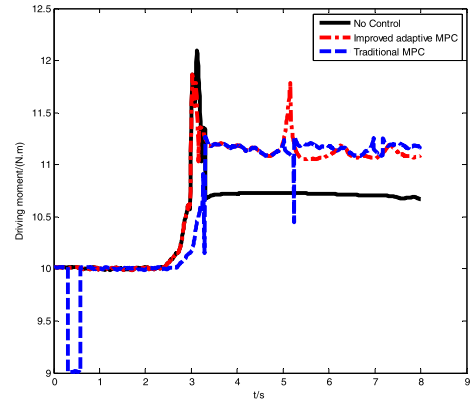

FIGURE 18. Change curve of the driving torque of the right front wheel under the step steering condition.

FIGURE 19. Change curve of the driving torque of the left rear wheel under the step steering condition.

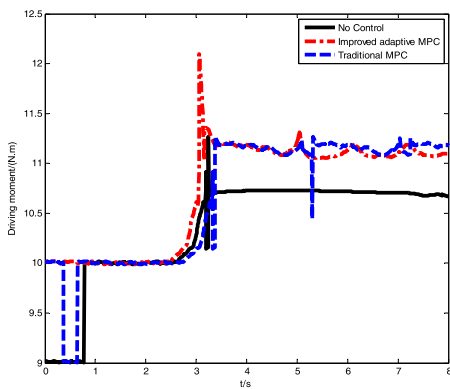**FIGURE 20.** Change curve of the driving torque of the right rear wheel under the step steering condition.

FIGURE 21. Experiment platform for the distributed electrically driven agricultural logistics.
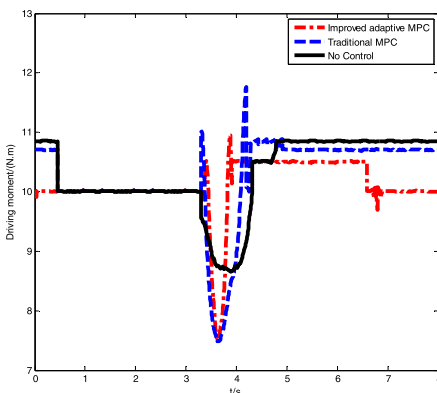
IV. EXPERIMENTAL PLATFORM CONSTRUCTION AND ROAD EXPERIMENTAL VERIFICATION OF AGRICULTURAL LOGISTICS OPERATION

The experiment platform of distributed electrically driven agriculture in the paper iss developed by our research group. This is a vehicle architecture developed based on the changing agricultural environment. The experimental platform adopts the four-wheel independent electric drive design, has the certain extension function and openness, and mainly includes the control system execution system data storage system. To satisfy the complicated and changeable requirements of agricultural operation, the platform can adjust the ground gap and wheelbase and realize the automation and visualization of the chassis. The experiment platform of distributed electrically driven agricultural logistics is shown in Fig. 21. Specific parameters of the experiment platform are shown in Table 4.

In the study, the agricultural vehicle logistics experimental platform for research is four-wheel independent drive, and each wheel is individually driven by a servo motor through a deceleration mechanism. The functional composition principle of each system of the experimental test platform is shown in Fig. 22.

the steering, and the driving torque of the outer drive wheel instantly increases and is sufficient to ensure complete steering. Compared to the traditional MPC control, the improved adaptive MPC control response to the driving force is timelier, and the effect is better.
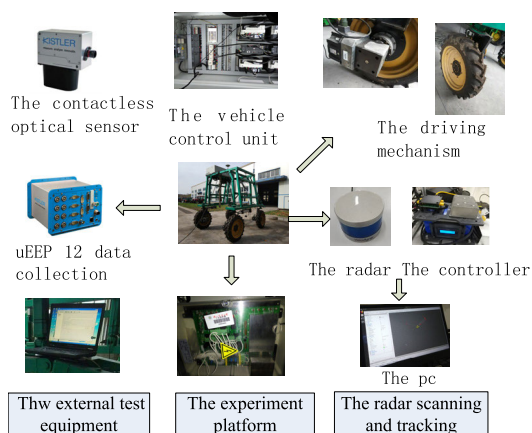
TABLE 4. Parameters of the 4-WID drive high-clearance vehicle.

Parameter	Value	Parameter	Value
Weight	1.2 t	Wheel tread	1.8-2.8 m
Ground clearance	2.5-3.0 m	Wheelbase	2.4 m
Maximum speed	18 km/h	Wheel diameter	0.96 m
Total power	20 KW		

FIGURE 22. Functional composition principle of each system of the experimental test platform.

FIGURE 23. GPS data transmission flow chart.

A. MAIN BODY OF THE EXPERIMENTAL PLATFORM

The drive motor is a Panasonic A52 series flat servo motor. A GPS receiving system is used for the real-time speed measurement. The model of the remote controller is LAMP-1000A, and an external antenna is applied to receive the signal. The functional composition principle of each system of the experimental test platform is shown in Fig. 22.

In the paper, GPS is used to measure the speed. The selected GPS is mainly divided into lithium battery, receiver, butterfly antenna and digital station.

The data collection and analysis software is MCGS (Beijing Kunlun Tongtai Co., LTD). The main function of MCGS is to collect field data, and it can process front-end data and control.
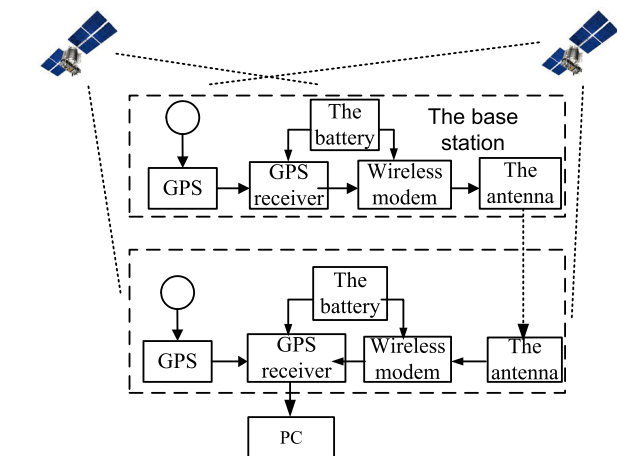
B. EXTERNAL TEST SYSTEM

To verify the control effect of the proposed control strategy in the vehicle driving state, the vehicle running state observation equipment is installed on the agricultural vehicle platform for data collection and analysis.

The UEEP 12 data acquisition and analysis system is used for the vehicle longitudinal and transverse dynamic performance test, and it can connect to a tablet or laptop to provide a new platform for online vehicle testing. In addition, UEEP 12 has the advantages of simultaneously collecting various signal data, compact size and operating temperature expandable range.

A Correvit S-motion biaxial sensor is used for the longitudinal and transverse dynamic testing of contactless vehicles.

C. EXPERIMENTAL SITE AND WORKING CONDITIONS

In the study, the experimental site is the open site of Jiangsu agricultural machinery testing and appraisal station. The experimental site is a grassy hard earth pavement, as shown in Fig. 24. Continuous steering experiments and step steering experiments are performed.

FIGURE 24. Test site.

The hard soil pavement is generally covered with weeds and mostly grassland pavement. The optimum slip rate of hard grassland pavement is 5.6-7.7%. First, the data collection is performed by making the agricultural logistics vehicles walk freely; then, adhesion coefficient μ is obtained using the adhesion coefficient estimation model, and its value is 0.76.

1) CONTINUOUS STEERING EXPERIMENT

The target vehicle performs continuous steering experiments at the test site. The vehicle speed is 20 km/h; we maintain and complet the test at this speed. As shown in Figs. 25-28, both traditional MPC control and improved adaptive MPC
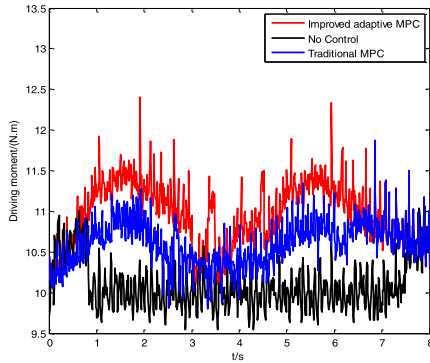
FIGURE 25. Change curve of the driving torque of the left front wheel obtained by the road experiment under the continuous steering condition.
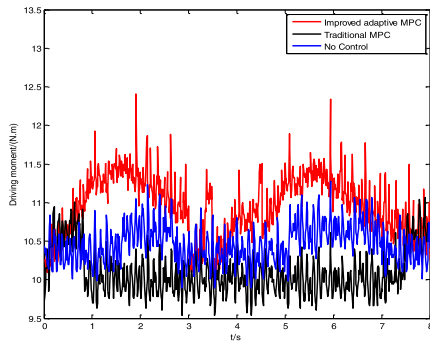

FIGURE 26. Change curve of the driving torque of the right front wheel obtained by the road experiment under the continuous steering condition.
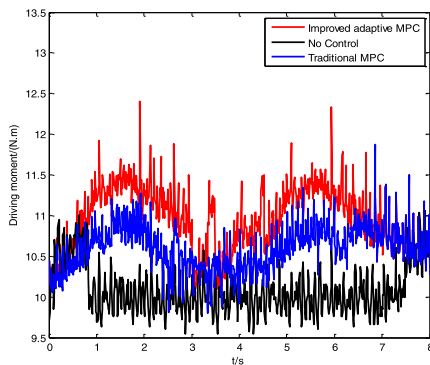

FIGURE 27. Change curve of the driving torque of the left rear wheel obtained by the road experiment under the continuous steering condition.

FIGURE 28. Change curve of the driving torque of the right rear wheel obtained by the road experiment under the continuous steering condition.

FIGURE 29. Vehicle trajectory without control in the continuous steering condition.

FIGURE 30. Vehicle trajectory under traditional MPC control in the continuous steering condition.

FIGURE 31. Vehicle trajectory under improved adaptive MPC control in the continuous steering condition.

control can adjust the driving torque of the left and right driving wheels according to the driving conditions. They can change the driving torque of the left and right driving wheels so that the target vehicle can keep the steering path in a timely and stable manner to avoid path deviation. Moreover, the improved adaptive MPC can more smoothly adjust the driving torque of the driving wheel to more fully steer it. Thus, the control effect is better. Figs. 29-31 show the vehicle trajectory of three different control strategies under the continuous steering condition: without control, under traditional MPC control, and under improved adaptive MPC
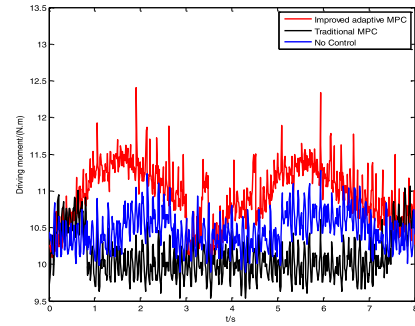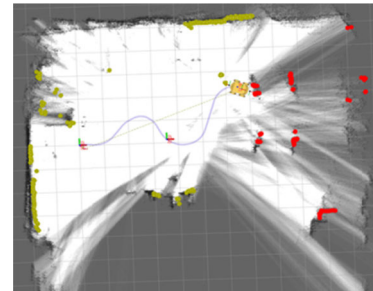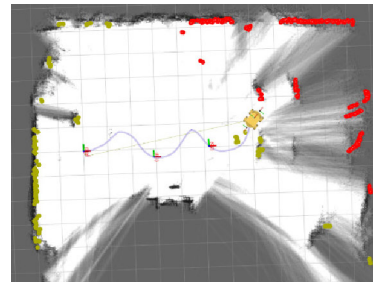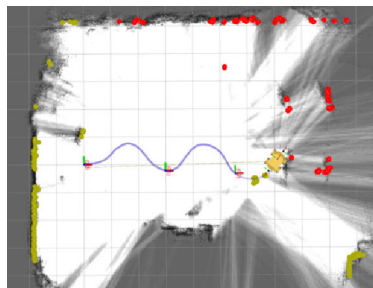
control, respectively. As shown in Figs. 29-31, when there is no control, the driving trajectory deviates from the predetermined trajectory in the second half of the operation, and the continuous steering condition is not completed. Although the
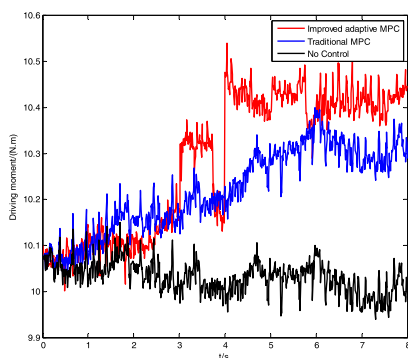
FIGURE 32. Change curve of the driving torque of the left front wheel obtained by the road experiment under the step steering condition.
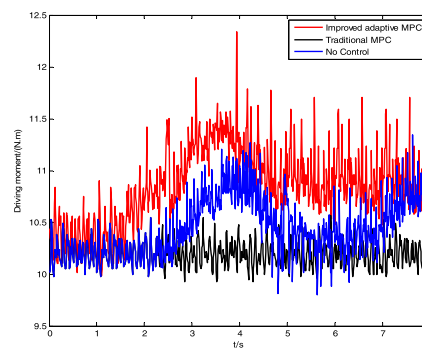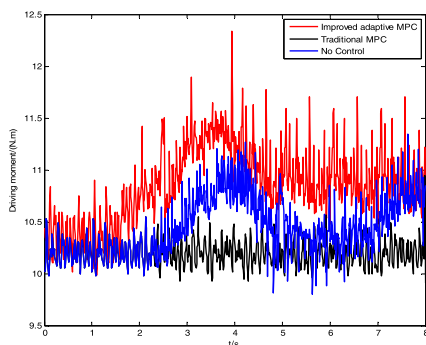

FIGURE 33. Change curve of the driving torque of the right front wheel obtained by the road experiment under the step steering condition.
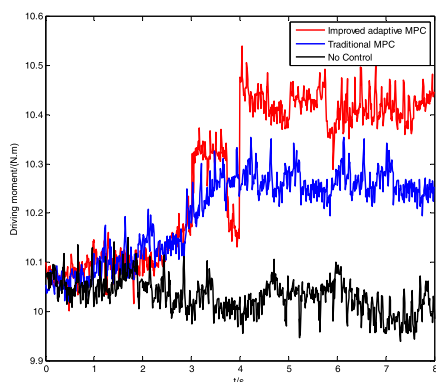

FIGURE 34. Change curve of the driving torque of the left rear wheel obtained by road experiment under the step steering condition.

conventional MPC control can complete the steering condition according to the predetermined trajectory, the trajectory appears astringent and not sufficiently continuous during the steering process. With the improved adaptive MPC control, the steering is smooth and continuous. Thus, the improved adaptive MPC control has the best control effect.

2) STEP STEERING EXPERIMENT
The target vehicle performs the step steering experiment at the test site with a vehicle speed of 20 km/h and maintains and completes the test at this speed. As shown in Figs. 32-35,
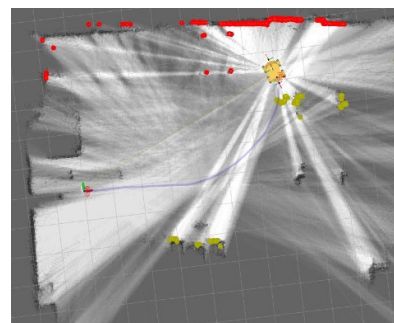

FIGURE 35. Change curve of the driving torque of the left rear wheel obtained by the road experiment under the step steering condition.

FIGURE 36. Vehicle trajectory without control in the step steering condition.
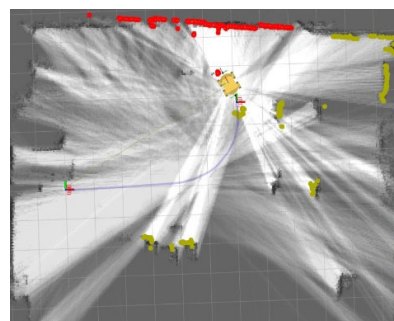
FIGURE 37. Vehicle trajectory under traditional MPC control in the step steering condition.

the traditional MPC control and improved adaptive MPC control can adjust the torque of the left and right driving wheels in time, so that the agricultural vehicles can better complete step steering, and the improved adaptive MPC control is better. Figs. 36-38 show the vehicle step steering trajectory under three different control strategies in the step steering condition: without control, under the control of traditional MPC, and under the control of improved adaptive MPC, respectively. As shown in Figs. 36-38, when there is no control, the vehicle can not complete the step steering as required, and the driving trajectory deviates from the preset trajectory. Although the conventional MPC control can complete step steering, the steering radius is too large to fully satisfy the mobility requirements of agricultural vehicles. With the
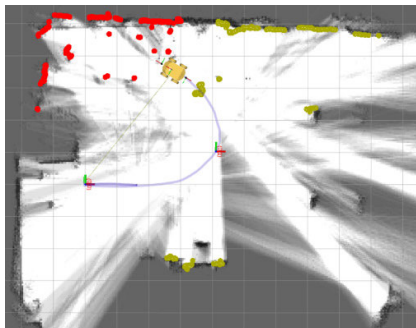
FIGURE 38. Vehicle trajectory under improved adaptive MPC control in the step steering condition.

improved adaptive MPC control, the steering radius is small, and the steering manoeuvrability is good. Thus, the improved adaptive MPC control has the best control effect.

V. CONCLUSION

To improve the driving performance of distributed electrically driven unmanned agricultural logistics vehicles, a driver coordination control strategy based on MPC and improved adaptive MPC is proposed in the current paper. Simulations of the control system and real vehicle experiment are completed. The obtained results are as follows. With the characteristics of independent four-wheel drive control and rapid torque response, the distributed electric vehicle can achieve faster yaw response and expand the stability range of the vehicle. The high accuracy and robustness of the model make it suitable for the lateral stability control of the distributed electrically driven agricultural logistics vehicles. Based on the effect of external interference and various uncertainties on the accuracy of the nonlinear prediction model, the model parameter adaptive estimator is designed. The model parameter adaptive estimator realizes the online adjustment of the parameter set of the prediction model, which can improve the robustness of the control system and ensure the asymptotic stability of the system. The agricultural logistics vehicle experimental platform built in the paper can realize the tracking and scanning of the actual scene target and site obstacle. Thus, it can provide technical support for the operation of intelligent agricultural logistics, and provide a foundation for the subsequent path optimization and analysis of the logistics platform.

REFERENCES

[1] H. Peng, W. Wang, C. Xiang, L. Li, and X. Wang, "Torque coordinated control of four in-wheel motor independent-drive vehicles with consideration of the safety and economy," *IEEE Trans. Veh. Technol.*, vol. 68, no. 10, pp. 9604–9618, Oct. 2019.

[2] K. Kaur, N. Kumar, and M. Singh, "Coordinated power control of electric vehicles for grid frequency support: MILP-based hierarchical control design," *IEEE Trans. Smart Grid*, vol. 10, no. 3, pp. 3364–3373, May 2019.

[3] H. Zhou, F. Jia, H. Jing, Z. Liu, and L. Guvenc, "Coordinated longitudinal and lateral motion control for four wheel independent motor-drive electric vehicle," *IEEE Trans. Veh. Technol.*, vol. 67, no. 5, pp. 3782–3790, May 2018.

[4] Y. Luo, T. Chen, S. Zhang, and K. Li, "Intelligent hybrid electric vehicle ACC with coordinated control of tracking ability, fuel economy, and ride comfort," *IEEE Trans. Intell. Transp. Syst.*, vol. 16, no. 4, pp. 2303–2308, Aug. 2015.

[5] K. Kondo, S. Sekiguchi, and M. Tsuchida, "Development of an electrical 4WD system for hybrid vehicles," SAE Tech. Paper 2002-01-1043, 2002.

[6] X. Zeng, Y. Wang, D. Song, L. Zhu, G. Tian, and Z. Li, "Coordinated control algorithm of a dual motor for an electric variable transmission hybrid system," *IEEE Access*, vol. 6, pp. 35669–35682, 2018.

[7] Y. Dai, Y. Luo, and W. Chu, "Optimum tyre force distribution for four-wheel-independent drive electric vehicle with active front steering," in *Proc. Int. Symp. Adv. Vehicle Control*, Seoul, South Korea, Sep. 2012, pp. 145–152.

[8] G. Tian, H. Zhang, M. Zhou, and Z. Li, "AHP, gray correlation, and TOPSIS combined approach to green performance evaluation of design alternatives," *IEEE Trans. Syst., Man, Cybern. Syst.*, vol. 48, no. 7, pp. 1093–1105, Jul. 2018.

[9] L. Xiong, Z. Yu, Y. Wang, C. Yang, and Y. Meng, "Vehicle dynamics control of four in-wheel motor drive electric vehicle using gain scheduling based on tyre cornering stiffness estimation," *Vehicle Syst. Dyn.*, vol. 50, no. 6, pp. 831–846, Jun. 2012.

[10] L. Chen, T. Chen, X. Xu, Y. Cai, H. Jiang, and X. Sun, "Multi-objective coordination control strategy of distributed drive electric vehicle by orientated tire force distribution method," *IEEE Access*, vol. 6, pp. 69559–69574, 2018.

[11] T. Oliveira, A. P. Aguiar, and P. Encarnacao, "Moving path following for unmanned aerial vehicles with applications to single and multiple target tracking problems," *IEEE Trans. Robot.*, vol. 32, no. 5, pp. 1062–1078, Oct. 2016.

[12] Q. Chen, Y. Sun, M. Zhao, and M. Liu, "A virtual structure formation guidance strategy for multi-parafoil systems," *IEEE Access*, vol. 7, pp. 123592–123603, 2019.

[13] G. Tian, Y. Ren, Y. Feng, M. Zhou, H. Zhang, and J. Tan, "Modeling and planning for dual-objective selective disassembly using AND/OR graph and discrete artificial bee colony," *IEEE Trans. Ind. Informat.*, vol. 15, no. 4, pp. 2456–2468, Apr. 2019.

[14] G. Tian, N. Hao, M. Zhou, W. Pedrycz, C. Zhang, F. Ma, and Z. Li, "Fuzzy grey choquet integral for evaluation of multicriteria decision making problems with interactive and qualitative indices," *IEEE Trans. Syst., Man, Cybern. Syst.*, early access, Apr. 12, 2019, doi: 10.1109/TSMC.2019.2906635.

[15] W. Tian, M. Lauer, and L. Chen, "Online multi-object tracking using joint domain information in traffic scenarios," *IEEE Trans. Intell. Transp. Syst.*, vol. 21, no. 1, pp. 374–384, Jan. 2020.

[16] M. Hajiaghaei-Keshteli, H. Mohammadzadeh, N. Sahebjamnia, and A. M. Fathollahi-Fard, "New approaches in metaheuristics to solve the truck scheduling problem in a cross-docking center," *Int. J. Eng.-Trans. B, Appl.*, vol. 31, no. 8, pp. 1258–1266, Aug. 2018.

[17] A. Abdi, A. Abdi, A. M. Fathollahi-Fard, and M. Hajiaghaei-Keshteli, "A set of calibrated metaheuristics to address a closed-loop supply chain network design problem under uncertainty," *Int. J. Syst. Sci., Oper. Logistics*, vol. 24, pp. 1–18, May 2019.

[18] S. Bahadori-Chinibelagh, A. M. Fathollahi-Fard, and M. Hajiaghaei-Keshteli, "Two constructive algorithms to address a multi-depot home healthcare routing problem," *IETE J. Res.*, vol. 44, pp. 1–7, Jul. 2019.

[19] B. A. Guvenc, T. Bunte, D. Odenthal, and L. Guvenc, "Robust two degree-of-freedom vehicle steering controller design," *IEEE Trans. Control Syst. Technol.*, vol. 12, no. 4, pp. 627–636, Jul. 2004.

[20] Q. Zhang and Z. Liu, "A novel piecewise affine model for vehicle lateral dynamics," *IEEE Access*, vol. 6, pp. 78493–78502, 2018.

[21] Y. Ma and Y. Cai, "A fuzzy model predictive control based upon adaptive neural network disturbance observer for a constrained hypersonic vehicle," *IEEE Access*, vol. 6, pp. 5927–5938, 2018.

[22] X. Zan, Z. Wu, C. Guo, and Z. Yu, "A Pareto-based genetic algorithm for multi-objective scheduling of automated manufacturing systems," *Adv. Mech. Eng.*, vol. 12, no. 1, pp. 1–15, Jan. 2020.

[23] Y. Feng, Z. Zhang, G. Tian, A. M. Fathollahi-Fard, N. Hao, Z. Li, W. Wang, and J. Tan, "A novel hybrid fuzzy grey TOPSIS method: Supplier evaluation of a collaborative manufacturing enterprise," *Appl. Sci.*, vol. 9, no. 18, p. 3770, Sep. 2019.

[24] A. M. Fathollahi-Fard, M. Ranjbar-Bourani, N. Cheikhrouhou, and M. Hajiaghaei-Keshteli, "Novel modifications of social engineering optimizer to solve a truck scheduling problem in a cross-docking system," *Comput. Ind. Eng.*, vol. 137, Nov. 2019, Art. no. 106103.

[25] A. M. Fathollahi-Fard, M. Hajiaghaei-Keshteli, G. Tian, and Z. Li, "An adaptive Lagrangian relaxation-based algorithm for a coordinated water supply and wastewater collection network design problem," *Inf. Sci.*, vol. 512, pp. 1335–1359, Feb. 2020.

[26] Y. Chen, C. Stout, A. Joshi, M. L. Kuang, and J. Wang, "Driver-assistance lateral motion control for in-wheel-motor-driven electric ground vehicles subject to small torque variation," *IEEE Trans. Veh. Technol.*, vol. 67, no. 8, pp. 6838–6850, Aug. 2018.

[27] Y. Feng, Y. Gao, G. Tian, Z. Li, H. Hu, and H. Zheng, "Flexible process planning and end-of-life decision-making for product recovery optimization based on hybrid disassembly," *IEEE Trans. Autom. Sci. Eng.*, vol. 16, no. 1, pp. 311–326, Jan. 2019.

[28] A. Tahouni, M. Mirzaei, and B. Najjari, "Novel constrained nonlinear control of vehicle dynamics using integrated active torque vectoring and electronic stability control," *IEEE Trans. Veh. Technol.*, vol. 68, no. 10, pp. 9564–9572, Oct. 2019.

[29] G. Hongyan, Z. Huayu, C. Hong, and L. Zhihai, "Vehicle yaw stability control based on MPC," in *Proc. 31st Chin. Control Conf.*, Heifei, China, Dec. 2012, pp. 1–6.

[30] G. Tian, M. Zhou, and P. Li, "Disassembly sequence planning considering fuzzy component quality and varying operational cost," *IEEE Trans. Autom. Sci. Eng.*, vol. 15, no. 2, pp. 748–760, Apr. 2018.

[31] A. M. Fatollahi-Fard, K. Govindan, M. Hajiaghaei-Keshteli, and A. Ahmadi, "A green home health care supply chain: New modified simulated annealing algorithms," *J. Cleaner Prod.*, vol. 240, Dec. 2019, Art. no. 118200.

[32] A. M. Fatollahi-Fard, M. Hajiaghaei-Keshteli, and R. Tavakkoli-Moghaddam, "The social engineering optimizer (SEO)," *Eng. Appl. Artif. Intell.*, vol. 72, pp. 267–293, Jun. 2018.

[33] N. Daroogheh, N. Meskin, and K. Khorasani, "Ensemble Kalman filters for state estimation and prediction of two-time scale nonlinear systems with application to gas turbine engines," *IEEE Trans. Control Syst. Technol.*, vol. 27, no. 6, pp. 2565–2573, Nov. 2019.

[34] D. Wang, W. Pedrycz, and Z. Li, "Granular data aggregation: An adaptive principle of the justifiable granularity approach," *IEEE Trans. Cybern.*, vol. 49, no. 2, pp. 417–426, Feb. 2019.

[35] V. Varadan, H. Leung, and E. Bosse, "Dynamical model reconstruction and accurate prediction of power-pool time series," *IEEE Trans. Instrum. Meas.*, vol. 55, no. 1, pp. 327–336, Feb. 2006.

[36] P. Zhou, H. Song, H. Wang, and T. Chai, "Data-driven nonlinear subspace modeling for prediction and control of molten iron quality indices in blast furnace ironmaking," *IEEE Trans. Control Syst. Technol.*, vol. 25, no. 5, pp. 1761–1774, Sep. 2017.

[37] A. Safaei and M. N. Mahyuddin, "Adaptive model-free control based on an ultra-local model with model-free parameter estimations for a generic SISO system," *IEEE Access*, vol. 6, pp. 4266–4275, 2018.

[38] H. Chun, M. Kim, J. Kim, K. Kim, J. Yu, T. Kim, and S. Han, "Adaptive exploration harmony search for effective parameter estimation in an electrochemical lithium-ion battery model," *IEEE Access*, vol. 7, pp. 131501–131511, Sep. 2019.

[39] M. J. Balas and S. A. Frost, "Robust adaptive model tracking for distributed parameter control of linear infinite-dimensional systems in Hilbert space," *IEEE/CAA J. Automatica Sinica*, vol. 1, no. 3, pp. 294–301, Jul. 2014.

[40] M. Partovibakhsh and G. Liu, "An adaptive unscented Kalman filtering approach for online estimation of model parameters and state-of-charge of lithium-ion batteries for autonomous mobile robots," *IEEE Trans. Control Syst. Technol.*, vol. 23, no. 1, pp. 357–363, Jan. 2015.

[41] D. Q. Dang, M. S. Rafaq, H. H. Choi, and J.-W. Jung, "Online parameter estimation technique for adaptive control applications of interior PM synchronous motor drives," *IEEE Trans. Ind. Electron.*, vol. 63, no. 3, pp. 1438–1449, Mar. 2016.

[42] W. Li, F. Duan, and C. Xu, "Design and performance evaluation of a simple semi-physical human-vehicle collaborative driving simulation system," *IEEE Access*, vol. 7, pp. 31971–31983, 2019.

[43] D. Zhang, G. Liu, H. Zhou, and W. Zhao, "Adaptive sliding mode fault-tolerant coordination control for four-wheel independently driven electric vehicles," *IEEE Trans. Ind. Electron.*, vol. 65, no. 11, pp. 9090–9100, Nov. 2018.

[44] R.-H. Zhang, Z.-C. He, H.-W. Wang, F. You, and K.-N. Li, "Study on self-tuning tyre friction control for developing main-servo loop integrated chassis control system," *IEEE Access*, vol. 5, pp. 6649–6660, 2017.

[45] D. Kim, S. Hwang, and H. Kim, "Vehicle stability enhancement of four-wheel-drive hybrid electric vehicle using rear motor control," *IEEE Trans. Veh. Technol.*, vol. 57, no. 2, pp. 727–735, Mar. 2008.

[46] D. Yin, N. Sun, and J.-S. Hu, "A wheel slip control approach integrated with electronic stability control for decentralized drive electric vehicles," *IEEE Trans. Ind. Informat.*, vol. 15, no. 4, pp. 2244–2252, Apr. 2019.

[47] Y. Jiang, W. Deng, J. Wu, S. Zhang, and H. Jiang, "Adaptive steering feedback torque design and control for driver-vehicle system considering driver handling properties," *IEEE Trans. Veh. Technol.*, vol. 68, no. 6, pp. 5391–5406, Jun. 2019.

[48] C. Sentouh, A.-T. Nguyen, M. A. Benloucif, and J.-C. Popieul, "Driver-automation cooperation oriented approach for shared control of lane keeping assist systems," *IEEE Trans. Control Syst. Technol.*, vol. 27, no. 5, pp. 1962–1978, Sep. 2019.

[49] Y. Koh, H. Her, K. Yi, and K. Kim, "Integrated speed and steering control driver model for vehicle-driver closed-loop simulation," *IEEE Trans. Veh. Technol.*, vol. 65, no. 6, pp. 4401–4411, Jun. 2016.

[50] A.-T. Nguyen, C. Sentouh, and J.-C. Popieul, "Driver-automation cooperative approach for shared steering control under multiple system constraints: Design and experiments," *IEEE Trans. Ind. Electron.*, vol. 64, no. 5, pp. 3819–3830, May 2017.

XUESHENG ZHOU received the B.S. degree in vehicle engineering from the Shandong University of Technology, Zibo, China, in 2013, and the M.S. degree from the Transportation College, Northeast Forestry University, China, in 2015. He is currently pursuing the Ph.D. degree with Nanjing Agricultural University.
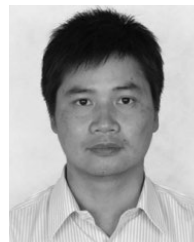
JUN ZHOU received the Ph.D. degree from Nanjing Agricultural University, China, in 2003. He is currently a Professor with Nanjing Agricultural University. His research interests include agricultural robots and precision agricultural equipment.